ACS Sustainable Chemistry & Engineering

Research Article

pubs.acs.org/journal/ascecg

Photocatalytic Hydrogen Production from Aqueous Na_2S + Na_2SO_3 Solution with B-Doped ZnO

Paramasivan Gomathisankar,*[,†] Katsumasa Hachisuka,[†] Hideyuki Katsumata,[†] Tohru Suzuki,[‡] Kunihiro Funasaka,[§] and Satoshi Kaneco*[,†,‡]

[†]Department of Chemistry for Materials, Graduate School of Engineering, and [‡]Environmental Preservation Center, Mie University, Tsu, Mie 514-8507, Japan

[§]Department of Urban Environment, Osaka City Institute of Public Health and Environmental Sciences, Osaka 543-0026, Japan

Supporting Information

ABSTRACT: Nonmetal (N and B) doped ZnOs were developed for hydrogen production from aqueous sacrificial anion, S^{2-}−SO_3^{2-}, solution. In the present work, N- and B-doped ZnO nanomaterials were successfully prepared by a simple, effective, high yield, and low cost mechanochemical combustion technique, with addition of urea or boric acid to a zinc acetate and oxalic acid mixture. The prepared oxides were characterized by X-ray diffraction (XRD), BET surface area analysis, X-ray photoelectron spectroscopy (XPS), scanning electron spectroscopy (SEM), UV−visible diffuse reflectance spectroscopy (UV-DRS), and photoluminescence spectroscopy (PL). The photocatalytic hydrogen production was observed with 880 μmol g^{-1} for undoped ZnO with 0.4 M Na_2S + 0.4 M Na_2SO_3 solution, due to in-situ formation of a ZnS/ZnO heterojunction. The doped ZnO materials had better activity than undoped ZnO. The photocatalytic H_2 evolution with B-doped ZnO (1730 μmol g^{-1}) was larger compared with those obtained with N-doped ZnO. The photocatalytic H_2 productions with B-doped ZnO were affected by parameters such as calcination temperature, calcination time, and doping concentrations. The B-doped ZnO demonstrated higher activity due to small particles size, large surface area, and reduction of electron−hole recombination.

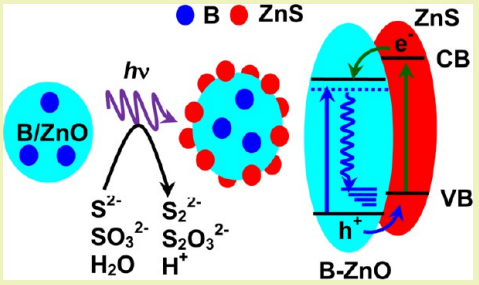

KEYWORDS: *Photocatalytic hydrogen generation, ZnO, Boron, Na_2S + Na_2SO_3, Heterojunction*

INTRODUCTION

Zinc oxide (ZnO) has been widely employed as a photocatalyst, UV light emitter, sensor, phosphor, and photovoltaic material, owing to its flexible preparation methods, high reactivity, low cost, and environmentally friendly features.[1−3] Although the electron transfer in ZnO is larger than that of TiO_2 even though the band gap value for both is almost the same,[3] there are only several reports concerning the photocatalytic H_2 production with ZnO, due to the drawback of its photocorrosion and dissolution. Therefore, the ZnO system needs suitable sacrificial agents in order to enhance the consumption of the photogenerated holes for minimizing the photocorrosion of ZnO and the electron hole pair recombination.

Since the extraction products, such as sulfides and sulfites of fossil energy resources now being produced in very large quantities, are the polluting byproducts in hydrogenation and flue-gas desulfurization processes at chemical plants, the photocatalytic reaction of hydrogen formation over sulfides from aqueous solution containing S^{2-} and SO_3^{2-} appears to become one of the powerful methods for the H_2 energy. Hence, because the decomposition of sulfide and sulfite ions consumes lower energy for splitting of water, it could be realized as a sacrificial agent in the photocatalytic H_2 production on semiconductors.[4−6]

In recent years, nonmetals have been used in semiconductors to modify band gap position, facilitate charge rectification, and improve carrier separation for photocatalytic hydrogen generation.[7−13] Recently, the photocatalytic H_2 evolution systems containing N- and C-doped ZnO have been reported.[12,13] To the best of our knowledge, there are few reports on the photocatalytic H_2 production with B-doped ZnO. Herein, we reported the highly efficient B-doped ZnO photocatalyst for the hydrogen production from aqueous S^{2-} + SO_3^{2-} solution. The experimental parameters, such as calcination temperature, calcination time, and doping concentrations, were optimized.

EXPERIMENTAL SECTION

Chemicals and Materials. Zinc acetate dehydrate (99.9%), oxalic acid (98%), boric acid (99.5%), urea (99%), sodium sulfide nonahydrate (98%), and sodium sulfite (97%) were obtained from Wako Pure Chemical Industries, Ltd. and were used as received without further purification. As the reference, commercial photocatalyst ZnO was purchased from Sigma-Aldrich (BET specific surface area 15−25 m^2/g, mean particle size 50−70 nm). Laboratory pure water was obtained

Received: March 4, 2013
Revised: May 2, 2013
Published: May 21, 2013

from an ultrapure water system (Advantec MFS Inc., Tokyo, Japan) resulting in a resistivity >18 MΩ cm.

Preparation of Photocatalyst. In a typical synthesis, 2.195 g of zinc acetate dihydrate and 1.512 g of oxalic acid were taken in agate mortar and the mixture was ground for 10 min in order to obtain a paste of zinc oxalate dihydrate and acetic acid. The existence of acetic acid was confirmed by its typical smell. The loss of acetic acid byproduct in the form of fumes became a driving force for the reaction. Urea was added to the above paste as a source of nitrogen, and the grinding process was continued for the next 10 min to obtain zinc oxalate−urea precursor. The same procedure was repeated with boric acid as a source of boron to obtain zinc oxalate−boric acid precursor. The N- and B-doped zinc oxide crystallites were obtained by calcination of precursor powders at the temperature of 300−900 °C under an air atmosphere. The undoped ZnO was also synthesized by calcination of a paste of zinc oxalate and acetic acid for the comparison.

Characterization of Photocatalyst. The powder X-ray diffractometer (XRD, RIGAKU Ultima IV, sample horizontal type) was used in order to record the diffraction patterns of photocatalysts employing Cu Kα radiation of wavelength 0.15406 nm with tube current of 50 mA at 40 kV in 2θ angle range from 10° to 80° with a scan speed of 4°/min and a step size of 0.02°. The specific surface areas of catalysts were determined by the three points BET method with N_2 adsorption−desorption isotherms (Quantachrome Instruments, Autosorb-1-C, chemisorption−physisorption analyzer, USA). A Hitachi S-4000 scanning electron microscope (SEM) was employed to observe the morphologies of oxides. The diffuse reflectance spectra (DRS) of photocatalysts were recorded over a range of 200−850 nm with a Shimadzu UV-2450 UV/vis system equipped with an integrating sphere diffuse reflectance accessory using the reference material $BaSO_4$. Photoluminescence (PL) spectra of oxide powders were measured at room temperature using a Shimadzu RF-5300PC system equipped with solid sample holder.

Photocatalytic Hydrogen Production. The pyrex column vessel reactor (inner volume: 55.6 mL) was used for the photocatalytic production of hydrogen from aqueous Na_2S−Na_2SO_3 solution. The pyrex glass cuts off all wavelength below 300 nm. Typically, 20 mg of the photocatalysts were added to 30 mL of aqueous Na_2S−Na_2SO_3 solution in the photoreactor. A xenon lamp (500 W, UXL-500D-O) was applied as light source, which was positioned on the side of photoreactor. The light intensity was measured by a UV radio meter with a sensor of 320−410 nm wavelengths (UVR-400, Iuchi Co., Osaka, Japan), and the value was 1.0 mW/cm^2. The photocatalysts were continuously dispersed in the aqueous Na_2S−Na_2SO_3 solution by a magnetic stirrer during the irradiation. The temperature of the suspension in the photoreactor was kept constant at 50 °C by the hot stirrer. The irradiation time was 3 h. The hydrogen product from the aqueous solution was analyzed by gas chromatography (GL Sciences, GC-3200) with a thermal conductivity detector (TCD). The stainless column (4 m long, 2.17 mm i.d.) packed with Molecular Sieve 5A was used for the separation. The carrier gas was high purity argon gas. The temperature conditions of GC were 50 °C for injection, column, and detector.

RESULT AND DISCUSSIONS

Crystal Structure. Figure 1 illustrates the X-ray diffraction patterns (XRDs) of Sigma-, undoped, and doped ZnO. The XRDs of the undoped and doped ZnO samples matched that of Sigma-ZnO, and their peaks were identical with those of primitive hexagonal crystal structure for zincite [JCPDS 79-0205]. It was found from the results that the doping of N or B could not modify the basic crystal structure of ZnO. When differently sized atoms are substituted in the ZnO lattice, some lattice defects and distortion of the crystal lattice seems to occur.[14−17] The XRD result suggests that the incorporation of B atoms leads to a depression of the crystal growth along the *c*-axis. Therefore, the crystallinity of ZnO was highly deteriorated in the presence of boron doping. The XRD pattern of B/ZnO became broader and slightly shifted toward a high angle than those for N-doped and undoped ZnO. This was attributed to the fact that the partial replacement of O with B results in the shrinkage of some crystallite plane of ZnO structure which results into the disordering of their crystallites. On the other hand, due to the substitution of lower radii B^{3+} (27 pm) with higher radii Zn^{2+} (64 pm), the lattice parameters may be decreased.[15] The deteriorated crystallinity for ZnO can be attributed to the formation of stresses by ion size difference between zinc and boron and the segregation of dopants in the grain boundaries.

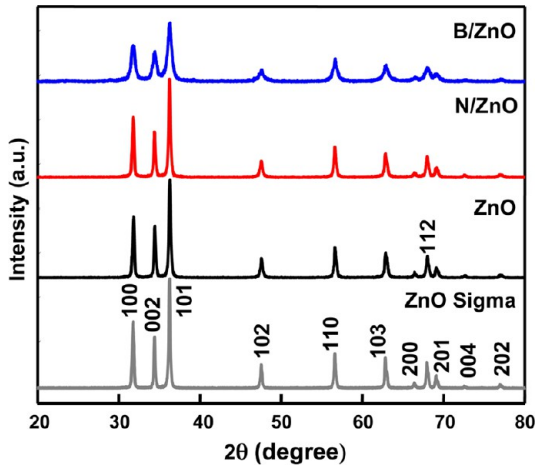

Figure 1. XRD patterns of Sigma-ZnO, undoped ZnO, 2 wt % N/ZnO, and 2 wt % B/ZnO.

The particle size of the oxides have been obtained from the full width at half maximum (FWHM) of the most intense peaks of the respective crystals using the Scherrer equation, $D = 0.9\lambda/\beta \cos\theta$, where D is the average crystallite size, λ is the X-ray wavelength, θ is the Bragg diffraction angle, and β is the full width at half-maximum. The crystal size of B-doped ZnO was smaller compared with those of the undoped one (Table 1). The crystal strains of doped ZnO were obtained from the slope (η) of the Williamson−Hall plot of $\beta \cos\theta$ versus 4sin θ, as shown in Supporting Information Figure S1. Positive slopes with 0.0005 and 0.0014 were observed for N- and B-doped ZnO, respectively, indicating the tensile strain for crystal ZnO. The physical parameters are shown in Table 1. Consequently, the B-doping influences showed the following characteristics: (i) broadening of XRD peaks, (ii) degradation in the crystallinity, (iii) reduction in crystallite size, (iv) smaller particle size, and (v) tensile strain.

The doping of boron could be confirmed by X-ray photoelectron spectroscopy (XPS). The XPS spectra of B-doped ZnO are illustrated in Figure S2 in the Supporting Information. The XPS peak observed at 1022.4 eV could be assigned to Zn $2p_{3/2}$ electrons. In the XPS of the O_{1s} region, the peaks at 530.9 eV were attributed to O^{2-} ion of ZnO and another at 532.2 eV is usually associated with the lower valent oxygen or adsorbed O_2.[18,19] Since the B_{1s} emission is very broad (FWHM approximately 1.31 eV), more than one form of boron had better be present. Inspection of the data exhibits the presence of high and low binding energy components. The high binding energy component (193.0 eV) can be attributable to B_2O_3. The low binding energy component (192.3 eV) might be owing to boron actually incorporated within ZnO lattice.[20]

Morphology. The morphologies of Sigma-, undoped, and doped ZnO were investigated by scanning electron spectroscopy (SEM), as shown in Figure 2. Sigma-ZnO gave the hexagonal rod shapes with the agglomeration of two or more particles. The

dx.doi.org/10.1021/sc400061w | ACS Sustainable Chem. Eng. 2013, 1, 982−988

Table 1. Summary of Physical Perameters

				lattice parameters				
catalyst	2θ for (101)	crystalline size,[a] nm	particle size,[b] nm	a, Å d_{hkl} 101	c, Å d_{hkl} 002	volume, Å^3	BET surface area, m^2/g	band gap, eV
ZnO (Sigma)	36.28	21.6	75	3.233	5.280	47.80	15−25	3.25
ZnO (prepared)	36.22	17.5	70	3.238	5.288	48.03	2.7	3.23
N/ZnO	36.26	16.9	45	3.235	5.283	47.89	6.0	3.26
B/ZnO	36.32	12.1	25	3.230	5.275	47.66	21.8	3.25

[a]Estimated from the Scherrer equation using the 101 peak. [b]Obtained from the SEM image.

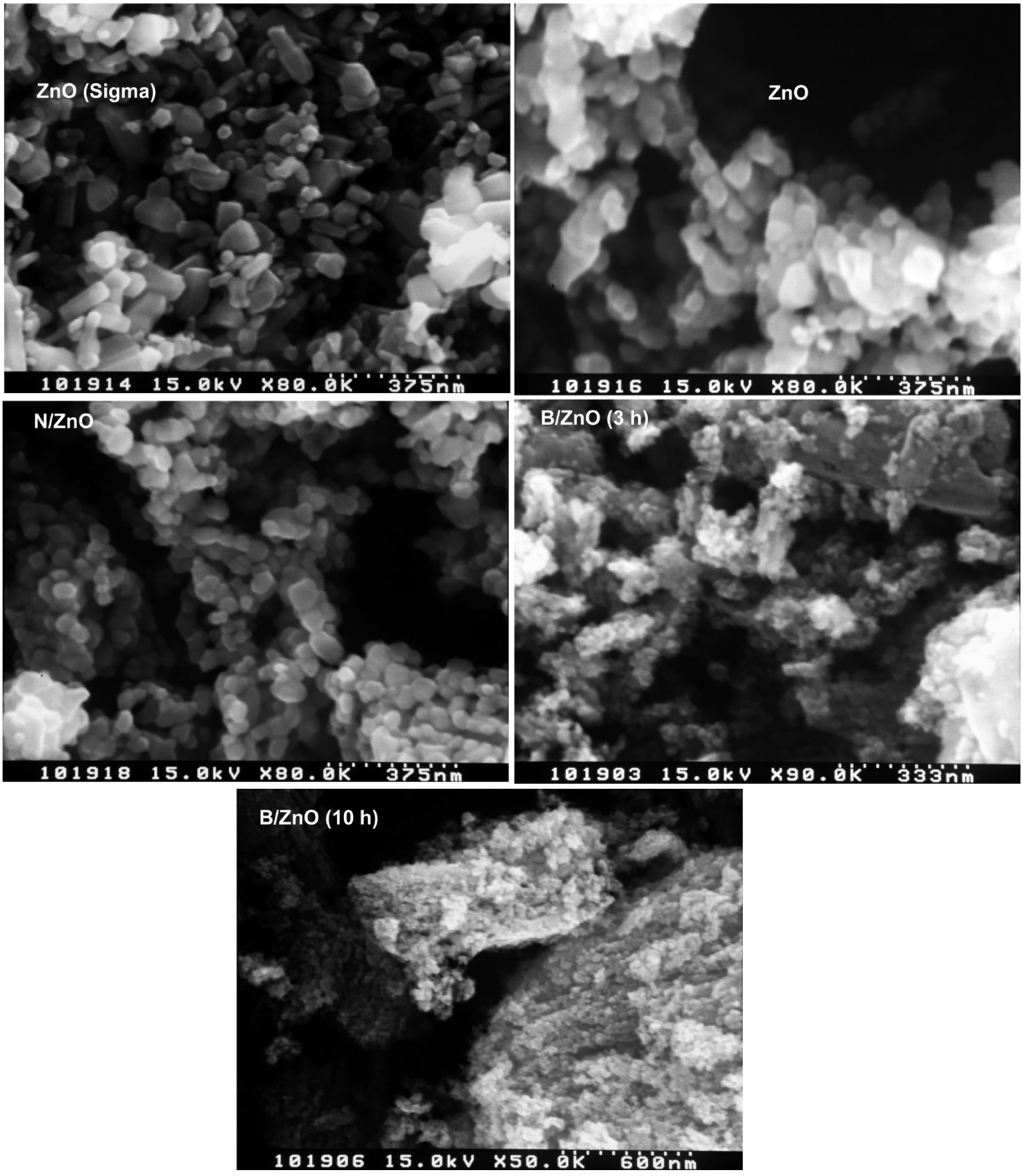

Figure 2. Morphological images of SEM for Sigma-ZnO, undoped ZnO, 2 wt % N/ZnO, and 2 wt % B/ZnO.

undoped and N-doped ZnO particles were agglomerated with primary particles having a few tens of nanometers. The SEM images for B-doped ZnO showed very fine spherical particles. The particle size of B/ZnO prepared for the calcination time 10 h

seems to become slightly larger relative to those obtained for 3 h. As a consequence, it could be confirmed from the SEM analysis that the B-doped ZnO exhibited the photocatalytic aspect consisting of very small particles.

Optical Property. The diffuse reflectance spectra of the undoped and doped ZnO samples were investigated, as depicted in Figure 3. The commercial Sigma-ZnO was also recorded for

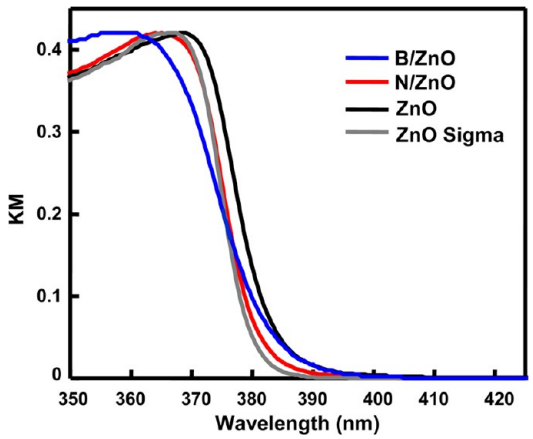

Figure 3. Diffuse reflectance spectra for Sigma-ZnO, undoped ZnO, 2 wt % N/ZnO, and 2 wt % B/ZnO.

the comparison. The reflectance data was converted to Kubelka–Munk equation which is expressed as $F(R) = (1 - R)^2/2R$. Synthesized oxides showed the similar light absorption in ultraviolet region as Sigma-ZnO. The band gap of the oxides were deduced from Tauc plot of $[F(R)h\nu]^2$ versus photon energy, and their values are presented in Table 1.

The room temperature photoluminescence (PL) spectra of Sigma-, undoped, and doped ZnO powder samples were recorded over the wavelength range 350–600 nm on the irradiation with xenon lamp excitation at different wavelengths. Figure 4 illustrates the PL spectra at excitation wavelengths of 335 and 350 nm, and the spectra observed at other excitation wavelengths are shown in Supporting Information Figure S3. In the PL spectra for ZnO, typically there are emission bands in the ultraviolet (UV) and visible (green, yellow, blue, and violet) regions.[21−23] It is generally accepted that the near UV emission of ZnO is closely related to the exciton transition from the localized level below the conduction band to the valence band or the exciton recombination. The emissions in the visible regions have been largely considered to be associated with the intrinsic or extrinsic defects in ZnO. The emission spectra of visible regions could depend on the excitation energy. All ZnO nanoparticles exhibit the usual band-edge emission with peak at 389 nm and the blue band emission with peak at 469 nm. It is estimated that the blue band emission is due to the recombination of electron in singly occupied oxygen vacancy with the photogenerated hole in the valence band. Recently, Zeng et al. have reported that the blue emissions are attributed to the transition from extended interstitial Zn states to the valence band.[21] When the low excitation energy was used (325 nm), the usual band−edge emission could not be obtained in the case of prepared ZnO. The band−edge and blue band emissions could be observed for the use of high excitation energy (350 nm). It was found from the PL data that the boron doping was very effective for the suppression of electron/hole recombination.

Effect of Calcination Temperature on the Photocatalytic H_2 Evolution with ZnO. The photocatalytic H_2 production of the doped ZnO were evaluated using xenon lamp in the aqueous 0.4 M Na_2S + 0.4 M Na_2SO_3 solution. Figure 5 shows the effect of calcination temperature on the photocatalytic hydrogen production with undoped and doped ZnO materials. The oxides were sintered at different temperatures

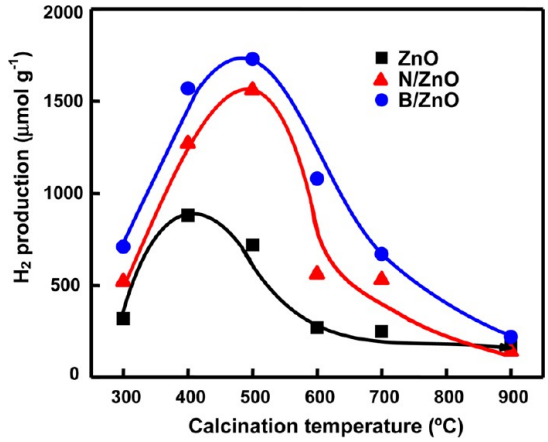

Figure 5. Effect of calcination temperature on the photocatalytic H_2 production from 0.4 M Na_2S + 0.4 M Na_2SO_3 solution. Calcination time 3 h, doping amount 2 wt %.

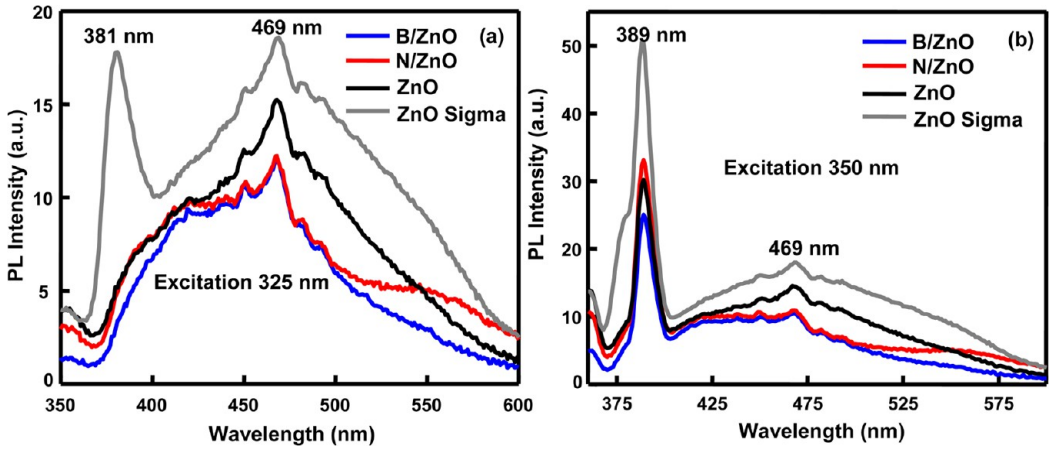

Figure 4. Photoluminescence spectra for Sigma-ZnO, undoped ZnO, 2 wt % N/ZnO, and 2 wt % B/ZnO. Excitation source: (a) 325, (b) 350 nm.

dx.doi.org/10.1021/sc400061w | ACS Sustainable Chem. Eng. 2013, 1, 982−988

such as 300, 400, 500, 600, 700, 800, and 900 °C and were tested for their photocatalytic H_2 production in aqueous Na_2S + Na_2SO_3 solution. The optimum calcination temperatures for undoped ZnO and B- or N-doped ZnO were 400 and 500 °C, respectively. The B-doped ZnO presented higher activity relative to those obtained with N-doped one.

Above 400−500 °C, the photocatalytic hydrogen production decreased with the calcination temperatures. It was reported previously that the crystallite size of the oxides increased with increasing the calcination temperatures.[16,17,24−26] Therefore, the reason for the decrease in the photocatalytic hydrogen production may be due to the larger particle size of ZnO. The best material for the photocatalytic H_2 production in aqueous Na_2S + Na_2SO_3 solution was the B-doped ZnO, which was sintered at 500 °C.

Effect of Calcination Time on the Photocatalytic H_2 Evolution with ZnO. The effect of calcination time on the photocatalytic hydrogen production using B-doped ZnO was investigated in the sacrificial S^{2-}−SO_3^{2-} solution. The results are illustrated in Figure 6. As the calcination time increased up to 3 h,

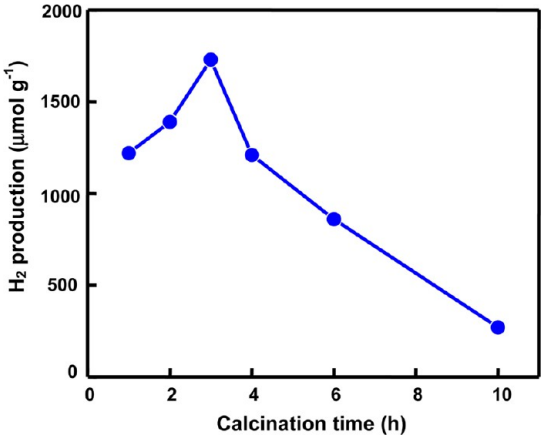

Figure 6. Effect of calcination time on the photocatalytic H_2 production from 0.4 M Na_2S + 0.4 M Na_2SO_3 solution. B doping 2 wt %, calcination temperature 500 °C.

the photocatalytic hydrogen production with B/ZnO increased gradually. After the calcination time of 3 h, the photocatalytic H_2 production turned from increase to decrease. The maximum hydrogen production was 1730 μmol g^{-1}, corresponded to the quantum efficiency 1.1%.

Effect of B-Doping Amount on the Photocatalytic H_2 Production. The influence of boron doping amounts on the photocatalytic hydrogen production was studied in the aqueous Na_2S−Na_2SO_3 solution. The results are depicted in Figure 7. The photocatalytic activity increased sharply with increasing the amount of boron doping into ZnO up to 2 wt %. Above the value, the photocatalytic hydrogen production almost became constant. The possible reason may be attributable to the trade-off between the decrease in particle size and the deterioration in crystallinity for ZnO.[16]

Reaction Mechanism. In order to better understand the photocatalytic process of hydrogen formation from an aqueous Na_2S−Na_2SO_3 solution, a possible mechanism based on the literature is shown in Figure 8.[4−6,14] The formed electrons and holes participate in redox processes at the semiconductor/solution interface. In the photoirradiation process, light is bombarded on the surface of the ZnO, and holes and electrons

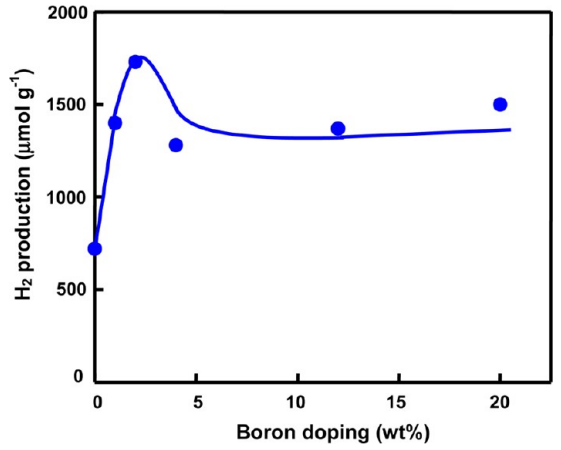

Figure 7. Effect of B-doping amount on the photocatalytic H_2 production from 0.4 M Na_2S + 0.4 M Na_2SO_3 solution. Calcination temperature 500 °C; calcination time 3 h.

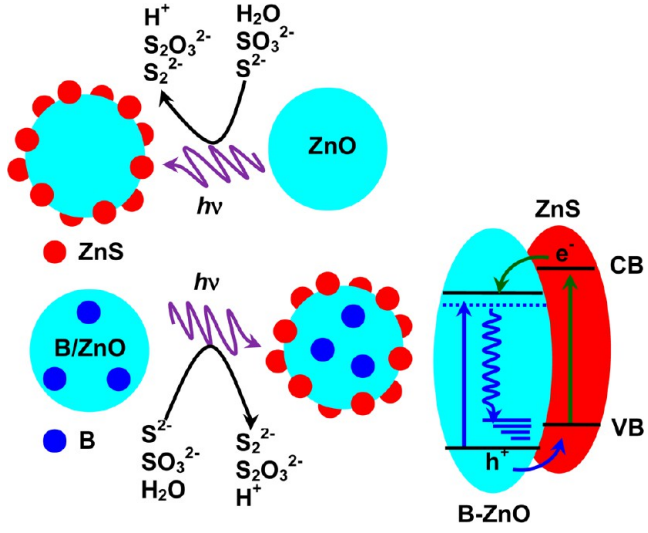

Figure 8. Graphical representation for the photocatalytic H_2 production.

are generated. At the same time, a hole reacts with water molecule to produce hydroxyl radical and H^+ ions. Na_2S + Na_2SO_3 solution acts as the hole scavenger. The surface of ZnO undergoes dissolution in alkaline sulfide solution for the formation of ZnS on the surface of ZnO particles.[27] From the X-ray diffraction analysis, the peak pattern for ZnO drastically changed after 3 h photoirradiation in the aqueous Na_2S/Na_2SO_3 solution, and the peaks were in perfect agreement with ZnS crystal structure (although the data is not shown). Probably, three different routes for scavenging the hole are possible (eqs 3, 4, and 6). The production of S_2^{2-} ions, which act as an optical filter and compete with reduction of protons, is efficiently suppressed by mixing SO_3^{2-} ions. SO_3^{2-} ions yields mainly thiosulfate ions. Finally, the formation of ZnS on the surface of ZnO appears to occur in the aqueous S^{2-} + SO_3^{2-} solutions.[13−15]

$$B/ZnO + h\nu \rightarrow B/ZnO(e_{CB}^- + h_{VB}^+) \quad (1)$$

$$2H_2O + 2e_{CB}^- \rightarrow H_2 + 2OH^- \quad (2)$$

$$SO_3^{2-} + H_2O + 2h_{VB}^+ \rightarrow SO_4^{2-} + 2H^+ \quad (3)$$

dx.doi.org/10.1021/sc400061w | ACS Sustainable Chem. Eng. 2013, 1, 982−988

$$2S^{2-} + 2h_{VB}^{+} \rightarrow S_2^{2-} \quad (4)$$

$$S_2^{2-} + SO_3^{2-} \rightarrow S_2O_3^{2-} + S^{2-} \quad (5)$$

$$SO_3^{2-} + S^{2-} + 2h_{VB}^{+} \rightarrow S_2O_3^{2-} \quad (6)$$

$$S_2O_3^{2-} + H^{+} \rightarrow HSO_3^{-} + S \quad (7)$$

$$S + 2e^{-} \rightarrow S^{2-} \quad (8)$$

$$Zn^{2+} + S^{2-} \rightarrow ZnS \quad (9)$$

$$Zn^{2+} + S + 2e^{-} \rightarrow ZnS \quad (10)$$

$$ZnS/B/ZnO + h\nu \rightarrow B/ZnO(e_{CB}^{-}) + ZnS(h_{VB}^{+}) \quad (11)$$

$$2H^{+} + B/ZnO(2e_{CB}^{-}) \rightarrow H_2 \quad (12)$$

The p- and n-type combined semiconductor (ZnS/B/ZnO) is formed by the photodeposition of ZnS on the surface of ZnO in the $Na_2S + Na_2SO_3$ solution (Figure 8). The conduction band (CB) of ZnS lies on a more negative potential than that of ZnO, whereas the valence band (VB) of ZnO is more positive than that of ZnS. The photogenerated electrons from the conduction band of ZnS nanoparticles can transfer to that of the ZnO and holes on the valence band of ZnO can move to that of the ZnS. The combination of ZnS with ZnO will create p−n type heterojunction semiconductor.

The role of B in the enhancement of the photocatalytic hydrogen production with ZnO in the sacrificial $S^{2-}-SO_3^{2-}$ anions is still under debate. A possible explanation is related to the replacement/substitution of B and their beneficial effect in reducing the recombination of photoexcited electrons and holes. At the same time, also the formation of small amounts of new B_2O_3, which could be confirmed by the XPS analysis, may be invoked to account for the relative high photoactivity of B-doped materials. Therefore, we prepared B-modified Sigma-ZnO in order to check the effect of the B_2O_3 formation. The B/Sigma-ZnO material was prepared by the deposition of B_2O_3 on the surface of ZnO. The photocatalytic H_2 production with B/Sigma-ZnO (370 μmol g^{-1}) was approximately one-fifth as small as those obtained with B-doped ZnO. Hence, the predominant influences of boron-doping seem to be smaller particle size and the lattice defect by replacement/substitution of B into ZnO.

CONCLUSIONS

In summary, the B-doped ZnO was applied into the photocatalytic H_2 evolution system containing the $S^{2-} + SO_3^{2-}$ solution. The optimum calcination temperature and time were 500 °C and 3 h, respectively. The best B-doping amount was 2 wt %. The maximum photocatalytic activity for H_2 evolution on B/ZnO (1730 μmol g^{-1} for 3 h) was about two times better compared with those obtained with undoped ZnO. The developed system may provide a strategy for the design of stable and inexpensive technologies for highly efficient H_2 production.

ASSOCIATED CONTENT

Supporting Information

Willamson−Hall plot, XPS, and PL. This material is available free of charge via the Internet at http://pubs.acs.org.

AUTHOR INFORMATION

Corresponding Author

*Tel.: +81-59-231-9427. Fax: +81-59-231-9427. E-mail: chemsankar79@gmail.com (P.G.), kaneco@chem.mie-u.ac.jp (S.K.).

Notes

The authors declare no competing financial interest.

ACKNOWLEDGMENTS

The present research was partly supported by Grant-in-Aid for Scientific Research (C) 24510096 from the Ministry of Education, Culture, Sports, Science, and Technology of Japan. Support was provided to P.G. as a Post Doctoral Research Fellow of The Public Foundation of Chubu Science and Technology Center. All experiments were conducted at Mie University. Any opinions, findings, conclusions, or recommendations expressed in this paper are those of the authors and do not necessarily reflect the view of the supporting organizations.

REFERENCES

(1) Karunakaran, C.; Rajeswari, V.; Gomathisankar, P. Optical, electrical, photocatalytic, and bactericidal properties of microwave synthesized nanocrystalline Ag-ZnO and ZnO. *Solid State Sci.* **2011**, *13* (5), 923−928.

(2) Gimenez, A. J.; Yanez-Limon, J. M.; Seminario, J. M. ZnO-Paper based photoconductive UV sensor. *J. Phys. Chem. C* **2011**, *115* (1), 282−287.

(3) Zhang, Q. F.; Dandeneau, C. S.; Zhou, X. Y.; Cao, G. Z. ZnO nanostructures for dye-sensitized solar cells. *Adv. Mater.* **2009**, *21* (41), 4087−4108.

(4) Tsuji, I.; Kato, H.; Kudo, A. Visible-Light-Induced H_2 Evolution from an aqueous solution containing sulfide and sulfite over a ZnS−$CuInS_2$−$AgInS_2$ solid-solution photocatalyst. *Angew. Chem., Int. Ed.* **2005**, *44* (23), 3565−3568.

(5) Park, H.; Kim, Y. K.; Choi, W. Reversing CdS preparation order and its effects on photocatalytic hydrogen production of CdS/Pt-TiO_2 hybrids under visible light. *J. Phys. Chem. C* **2011**, *115* (13), 6141−6148.

(6) Zhang, J.; Yu, J.; Zhang, Y.; Li, Q.; Gong, J. R. Visible light photocatalytic H_2- production activity of CuS/ZnS porous nanosheets based on photoinduced interfacial charge transfer. *Nano Lett.* **2011**, *11* (11), 4774−4779.

(7) Kitano, M.; Funatsu, K.; Matsuoka, M.; Ueshima, M.; Anpo, M. Preparation of nitrogen-substituted TiO_2 thin Film photocatalysts by the radio frequency magnetron sputtering deposition method and their photocatalytic reactivity under visible light irradiation. *J. Phys. Chem. B* **2006**, *110* (50), 25266−25272.

(8) Lin, C.; Chao, J.; Liu, C.; Chang, J.; Wang, F. Effect of calcination temperature on the structure of a Pt/TiO_2 (B) nanofiber and its photocatalytic activity in generating H_2. *Langmuir* **2008**, *24* (17), 9907−9915.

(9) Sreethawong, T.; Laehsalee, S.; Chavadej, S. Comparative investigation of mesoporous- and non-mesoporous-assembled TiO_2 nanocrystals for photocatalytic H_2 production over N-doped TiO_2 under visible light irradiation. *Int. J. Hydrogen Energy* **2008**, *33* (21), 5947−5957.

(10) Sakulkhaemaruethai, S.; Sreethawong, T. Synthesis of mesoporous-assembled TiO_2 nanocrystals by a modified urea-aided sol−gel process and their outstanding photocatalytic H_2 production activity. *Int. J. Hydrogen Energy* **2011**, *36* (11), 6553−6559.

(11) Sivaranjani, K.; Gopinath, C. S. Porosity driven photocatalytic activity of wormhole mesoporous $TiO_{2-x}N_x$ in direct sunlight. *J. Mater. Chem.* **2011**, *21* (8), 2639−2647.

(12) Bhirud, A. P.; Sathaye, S. D.; Waichal, R. P.; Nikam, L. K.; Kale, B. B. An eco-friendly, highly stable and efficient nanostructured p-type N-doped ZnO photocatalyst for environmentally benign solar hydrogen production. *Green Chem.* **2012**, *14* (10), 2790−2798.

(13) Lin, Y.; Hsu, Y.; Chen, Y.; Chen, L.; Chen, S.; Chen, K. Visible-light-driven photocatalytic carbon-doped porous ZnO nanoarchitectures for solar water-splitting. *Nanoscale* **2012**, *4* (20), 6515−6519.
(14) Qin, H.; Li, W.; Xia, Y.; He, T. Photocatalytic activity of heterostructures based on ZnO and N-doped ZnO. *ACS Appl. Mater. Interfaces* **2011**, *3* (8), 3152−3156.
(15) Gaikwad, R. S.; Bhande, S. S.; Mane, R. S.; Pawar, B. N.; Gaikwad, S. L.; Han, S.; Joo, O. Roughness-based monitoring of transparency and conductivity in boron-doped ZnO thin films prepared by spray pyrolysis. *Mater. Res. Bull.* **2012**, *47* (12), 4257−4262.
(16) Ilican, S.; Yakuphanoglu, F.; Caglar, M.; Caglar, Y. The role of pH and boron doping on the characteristics of sol gel derived ZnO films. *J. Alloys Compd.* **2011**, *509* (17), 5290−5294.
(17) Potti, P. R.; Srivastava, V. C. Comparative studies on structural, optical, and textural properties of combustion derived ZnO prepared using various fuels and their photocatalytic activity. *Ind. Eng. Chem. Res.* **2012**, *51* (23), 7948−7956.
(18) Mekasuwandumrong, O.; Pawinrat, P.; Praserthdam, P.; Panpranot, J. Effects of synthesis conditions and annealing post-treatment on the photocatalytic activities of ZnO nanoparticles in the degradation of methylene blue dye. *Chem. Eng. J.* **2010**, *164* (1), 77−84.
(19) Patil, A. B.; Patil, K. R.; Pardeshi, S. R. Enhancement of oxygen vacancies and solar photocatalytic activity of zinc oxide by incorporation of nonmetal. *J. Solid State Chem.* **2011**, *184* (12), 3273−3279.
(20) Dozzi, M. V.; Selli, E. Doping TiO_2 with p-block elements: Effects on photocatalytic activity. *J. Photochem. Photobiol. C* **2013**, *14*, 13−28.
(21) Zeng, H.; Duan, G.; Li, Y.; Yang, S.; Xu, X.; Cai, W. Blue luminescence of ZnO nanoparticles based on non-equilibrium processes: Defect origins and emission controls. *Adv. Funct. Mater.* **2010**, *20* (4), 561−572.
(22) Zhang, D. H.; Wang, Q. P.; Xue, Z. Y. Photoluminescence of ZnO films excited with light of different wavelength. *Appl. Surf. Sci.* **2003**, *207* (1−4), 20−25.
(23) Gao, X. D.; Li, X. M.; Yu, W. D. Rapid preparation, characterization, and photoluminescence of ZnO films by a novel chemical method. *Mater. Res. Bull.* **2005**, *40* (7), 1104−1111.
(24) Lu, J.; Zhang, Q.; Wang, J.; Saito, F.; Uchida, M. Synthesis of N-doped ZnO by grinding and subsequent heating ZnO-urea mixture. *Powder Technol.* **2006**, *162* (1), 33−37.
(25) Praserthdam, P.; Silveston, P. L.; Mekasuwandumrong, O.; Pavarajarn, V.; Phungphadung, J.; Somrang, P. A new correlation for the effects of the crystallite size and calcination temperature on the single metal oxides and spinel oxide nanocrystal. *Cryst. Growth Des.* **2004**, *4* (1), 39−43.
(26) Li, Y.; Ma, G.; Peng, S.; Lu, G.; Li, S. Boron and nitrogen co-doped titania with enhanced visible-light photocatalytic activity for hydrogen evolution. *Appl. Surf. Sci.* **2008**, *254* (21), 6831−6836.
(27) Arai, T.; Senda, S.; Sato, Y.; Takahashi, H.; Shinoda, K.; Jeyadevan, B.; Tohji, K. Cu-doped ZnS hollow particle with high activity for hydrogen generation from alkaline sulfide solution under visible light. *Chem. Mater.* **2008**, *20* (5), 1997−2000.